ACS APPLIED MATERIALS & INTERFACES

www.acsami.org

Research Article

Red Microalgal Sulfated Polysaccharide–Cu_2O Complexes: Characterization and Bioactivity

Nofar Yehuda, Yury Turkulets, Ilan Shalish, Ariel Kushmaro, and Shoshana (Malis) Arad*

Cite This: https://dx.doi.org/10.1021/acsami.0c17919

Read Online

ACCESS | Metrics & More | Article Recommendations | Supporting Information

ABSTRACT: The anion-exchange capacity of the cell-wall sulfated polysaccharide of the red microalga *Porphyridium* sp. can be exploited for the complexation of metal ions (e.g., Cu, Zn, Ag) to produce novel materials with new bioactivities. In this study, we investigated this algal polysaccharide as a platform for the incorporation of copper as Cu_2O. Chemical and rheological characterization of the Cu_2O–polysaccharide complex showed that the copper is covalently bound to the polysaccharide and that the complex exhibits higher viscosity and conductivity than the native polysaccharide. Examination of the complex's inhibitory activity against the bacteria *Acinetobacter baumannii*, *Pseudomonas aeruginosa*, *Escherichia coli*, *Staphylococcus aureus*, and *Bacillus subtilis* and the fungus *Candida albicans* revealed a relatively high antimicrobial activity, especially against *C. albicans* (92% growth inhibition) as compared to the polysaccharide and to Cu_2O alone. The antibiofilm activity was also found against *P. aeruginosa* PA14 and *C. albicans* biofilms. An atomic force microscopy examination of the surface morphology of the complex revealed needle-like structures (spikes), approximately 10 nm thick, protruding from the complex surface to a maximum height of 1000 nm, at a density of about 5000/μm^2, which were not detected in the native polysaccharide. It seems that the spikes on the surface of the Cu_2O–polysaccharide complex are responsible for the antimicrobial activities of the complex, that is, for disruption of microbial membrane permeability, leading to cell death. The study thus indicates that the superior qualities of the novel material formed by complexion of Cu_2O to the polysaccharide should be studied further for various biotechnological applications.

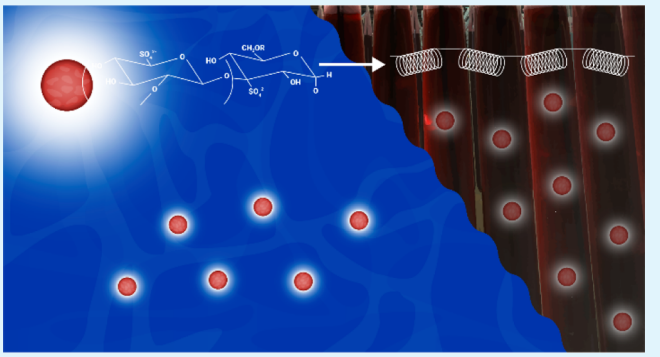

KEYWORDS: *Red microalgae, Porphyridium sp., Sulfated polysaccharide, Cu_2O, Antibacterial activity, Antibiofilm activity*

INTRODUCTION

The red microalgae, comprising a taxum of about eight genera, are morphologically the simplest of all the red algae. They are found in a range of different aquatic habitats, with some growing in fresh water and others growing in brackish or seawater. Reproduction is asexual, and in most species, the cells are brown as a result of their chlorophyll and phycoerythrin contents.[1] In studies of these microalgae, a great deal of work has been devoted to the genus *Porphyridium*, with both the ultrastructure[1] and the conditions for growth[2,3] being well documented.

The cells of the red microalga *Porphyridium* sp. are encapsulated within a sulfated polysaccharide, whose external part dissolves in the medium, thereby increasing its viscosity.[4] This sulfated polysaccharide is composed of 10 different sugars, of which the main ones are xylose, glucose, and galactose.[5] The sulfated polysaccharide has a molecular mass of $5–7 \times 10^6$ Da and is negatively charged due to the presence of glucuronic acid and half-ester sulfate groups.[5,6] The sulfate content in the polysaccharide varies between 6 and 7% w/v.[5] Aqueous solutions of the polysaccharide are stable over a wide range of temperatures (30–160 °C), pH values (2–9), and salinities, and solution viscosity appears to be unaffected by changes in the environment.[7,8] It has therefore been suggested that the sulfated cell-wall polysaccharide provides a buffer layer around the cells, protecting them not only against severe environmental conditions but also against bacteria, viruses, and fungi[7−9] by virtue of its activity in maintaining cell humidity and in free radical scavenging under conditions of high light. The cell-wall polysaccharide may also contribute to cellular ionic regulation by selective cation binding.[10] It is thus not surprising that the *Porphyridium* sp. cell-wall polysaccharide exhibits a variety of bioactivities, including antiviral,[11] anti-inflammatory,[12] antioxidant,[13] antibiofilm,[14] and bio-lubricant[15] activities. These unique qualities make it suitable for a

Received: October 6, 2020
Accepted: January 25, 2021

variety of industrial applications, including those in the cosmetics, pharmaceutical, and food industries (as a gelling, thickening, and stabilizing agent).

By virtue of its negative charge and its anion-exchange capacity,[16,17] it has been suggested that the polysaccharide can serve as a platform for metal incorporation as a means to produce new materials with synergistic metal−polysaccharide antimicrobial activities. For example, the complexation of the polysaccharide with zinc ions (as $ZnCl_2$) enhances its antibacterial activity compared with that of the native polysaccharide.[18] Similarly, an association of copper ions (as $CuCl_2$) with the polysaccharide prevents biofilm formation by modulating bacterial adhesion.[14] The applicative significance of the copper−polysaccharide interaction lies in the fact that microorganisms are extremely susceptible to copper, while copper is considered to be safe for external application on human skin, with a very low risk of adverse reactions.[19] Indeed, numerous investigations have been conducted regarding the possible use of copper as an antimicrobial agent.[20−22,35] These studies have shown that the bacterial toxicity of copper may be due to the displacement of essential metals from their native binding sites, interference with oxidative phosphorylation and the osmotic balance, and alterations of the conformational structure of nucleic acids, membranes, and proteins.[23] In microorganisms, including microalgae, metals can cause the formation of reactive oxygen species that interact with lipids, proteins, and nucleic acids, resulting in their degradation. As a protective response, the synthesis of chelating agents, such as phytochelatin or exopolymers, is increased.[24,25]

Studies of copper oxide—and other metals and metal oxides (silver, gold, palladium selenium, zinc oxide, and titanium dioxide)—in the form of nanoparticles have focused on their antifungal efficacy.[26−29] In particular, the role played by the surface composition of the nanoparticles in their antimicrobial activity has been studied.[30] Al-Awady et al.,[31] for example, developed polyelectrolyte-coated titania NPs with up to four layers of polyelectrolytes of alternating charge. A cationic outer layer (i.e., bare nanoparticles) was found to be a more effective antimicrobial than the anionic outer layer polyelectrolyte, probably by virtue of the increased adhesion of the cationic nanoparticles to the bacterial membrane.[31−33] It has been shown that the antibacterial activity of Cu_2O-based nanoparticles derives from copper-induced plasmid DNA degradation in a dose-dependent manner in both Gram-positive and Gram-negative bacteria.[32,34] Toxic effects of polymer-coated CuO nanoparticles have also been shown in the green microalga *Chlamydomonas reinhardtii*.[35] In addition, it has been shown that Cu administered as a hybrid−Cu−chitosan complex was similarly highly effective against fungi and different bacterial strains[36,37] even under anaerobic conditions (although Cu can be rapidly oxidized).[37,38] Moreover, Cu_2O has been widely used in hospitals as an antimicrobial agent, significantly reducing the occurrence of hospital-acquired infections and their costs.[39] It is important to note here that—alongside its antimicrobial activity—copper is also an essential micronutrient for organisms. Physiologically, copper exists in the form of ions, and in fungi such as *Candida albicans*, it is a functional component of various enzymes and chaperones.[40]

Recently, a different type of mechanism has been suggested for the antimicrobial activity of natural and bio-inspired materials that have a nano-spiked surface where the nano-topography spikes have been shown to physically rupture the microbial cell membrane of bacteria and fungi.[41−51] The antimicrobial activity of such natural and synthetic spikes after adhesion to the microbial cell membrane has been attributed to a number of different factors,[52] including the density and size of the spikes (ranging from 40 to 500 nm) and the rigidity of the microbial cell-wall (envelop architecture). However, the precise mechanism that leads to microbial cell death has not yet been elucidated conclusively.

The above studies provided the rationale for the current investigation in which we studied and characterized the bioactivity of a complex composed of the cell-wall sulfated polysaccharide of *Porphyridium* sp. and Cu_2O. It seems that the superior antibacterial and antifungal activities exhibited by the Cu_2O−polysaccharide complex were due to formation of spikes on the surface of the complex that led to mechanical damage to the microbial cell wall after adhesion of the complex to the microorganisms. It would thus appear that this complex has potential for development as a novel product that could be suitable for a variety of medical and cosmetic applications.

EXPERIMENTAL SECTION

Algal Growth and Polysaccharide Production. *Porphyridium* sp. (UTEX 637) obtained from the culture collection of the University of Texas at Austin was grown in artificial seawater.[3] Culture of the algal cells and isolation of the extracellular polysaccharide were performed as previously described.[53] Briefly, the cells were grown in polyethylene sleeves in the appropriate medium. The cultures were illuminated continuously with fluorescent cool-white lamps at an irradiance of 150 μE m^{-2} s^{-1} and aerated with sterile air containing 3% CO_2. Cells were harvested at the stationary phase of growth by continuous centrifugation (CEPA, Carl Padberg Zentrifugenbau GmbH, Lahr, Germany). The supernatant containing the dissolved polysaccharide was collected and filtered using crossflow filtration to remove salts and other metabolites (MaxCell hollow fiber microfiltration cartridge, pore size 0.45 μm, membrane area 2.5 m^2) and concentrated to 0.7% (w/v) polysaccharide. The resulting polysaccharide was sterilized in an autoclave and stored at 4 °C. The sugar content was determined using the phenol−sulfuric acid reaction.[54]

Complex Preparation. The Cu_2O−polysaccharide complex was prepared by directly adding Cu_2O (Fisher Scientific, Loughborough, UK) to 20 mL of a 0.7% (w/v) polysaccharide solution to give a final copper concentration of 500 ppm. The Cu_2O−polysaccharide complex was stirred gently with a magnetic stirrer for 24 h at room temperature and then sterilized by autoclaving.

Copper Concentration. The copper concentration in the Cu_2O−polysaccharide complex was evaluated by inductively coupled plasma optical emission spectrometry (SPECTRO ARCOS ICP-OES analyzer).

Viscosity. The viscosity of the polysaccharide solutions was determined with a Brookfield digital viscometer, 30 rpm at room temperature with a 31 cylindrical spindle (Brookfield AMETEK SC4-31).

Conductivity. The conductivity of the polysaccharide solutions was determined with a pH/mV/Cond./TDS/Temp. meter 86505 at room temperature.

Cyclic Voltammetry. A Metrohm 757 VA Computerize instrument was employed to obtain cyclic voltammograms of the Cu_2O−polysaccharide complex in an acetonitrile solution at room temperature (25 °C) under a nitrogen atmosphere, with lithium perchlorate as the supporting electrolyte. A glass carbon working electrode, a platinum auxiliary electrode, and an Ag/AgCl reference electrode were also used.

Rheology (G', G''). Dynamic viscoelastic characterization of the Cu_2O−polysaccharide complex (0.7% w/v polysaccharide with 500 ppm Cu) was determined by the frequency dependence of the storage and loss moduli, G' and G''. Measurements were carried out using a

https://dx.doi.org/10.1021/acsami.0c17919
ACS Appl. Mater. Interfaces XXXX, XXX, XXX−XXX

Table 1. Effect of the Addition of Copper on the Viscosity, Conductivity, and Zeta Potential of Cu_2O−Polysaccharide Complexes[a]

sample	copper added (ppm)	viscosity (cP)[b]	conductivity (μS)*	zeta potential (mV)*
Polysaccharide[c]	-	1830 ± 125	1,150 ± 20	−45 ± 3
Cu_2O−polysaccharide	250	1972 ± 220	2,532 ± 44	−47 ± 2
	500	2025 ± 110	2,857 ± 15	−48 ± 0
	750	2328 ± 124	3,235 ± 20	−49 ± 3

[a]The Cu_2O−polysaccharide complex was prepared by directly adding Cu_2O to the polysaccharide and stirring the mixture gently with a magnetic stirrer for 24 h at room temperature. [b]Values are means ± SD of three different experiments performed in triplicate. [c]Polysaccharide concentration in all samples was 0.7% (w/v) and the pH was 4.5.

Rheometer AR 2000 (TA Instruments) equipped with an extended temperature cell for temperature control and a stainless-steel parallel plate (d = 40 mm). The samples were held at room temperature for at least 20 min. After the temperature reached 25 °C, rheological tests were performed.

Fourier Transform Infrared Spectroscopy. Spectra were obtained on an iN-10 FTIR ThermoFisher Microscope spectrometer equipped with a narrow-band liquid-nitrogen-cooled MCT (Mercury Cadmium Telluride) detector. Samples of the Cu_2O−polysaccharide complex and the polysaccharide were lyophilized at −55 °C for 24 h in 96-well plates. The spectra were recorded in three areas per sample in the range of 4000−650 cm^{-1} at a 2 cm^{-1} resolution and 64 scans; the area of detection was 25 × 25 mm. The FTIR data were collected using OMNIC Picta software. Automatic baseline correction was used.

Scanning Electron Microscopy/Energy-Dispersive X-Ray Spectroscopy Analysis. The morphological properties of the Cu_2O−polysaccharide complex and the native polysaccharide were analyzed by SEM (FEI ESEM Quanta 200) at an accelerating voltage of 20 kV. In preparation for SEM scanning, 200 μL of samples was lyophilized at −55 °C for 24 h in 96-well plates. Then, the dried samples were attached to specimen holders with double-sided carbon tape and coated with a 20 nm layer of gold using the EMITECH K575x sputtering device (Emitech Ltd, UK).

Atomic Force Microscopy. Glass coverslips were immersed in 2.5 M HCl for 10 min and then rinsed first with ethanol (99.9%) and then with distilled water. Then, 10 μL of the Cu_2O−polysaccharide complex or the native polysaccharide was applied to the glass surface and dehydrated by autoclaving at 121 °C for 40 min. Topographical images of the pre-dried Cu_2O−polysaccharide complex and native polysaccharide were acquired on a Dimension-3100 microscope (Bruker). Samples were imaged at a scan rate of 0.5−1 Hz with a 512 × 512 pixel resolution in tapping mode. Several scans were carried out over a given surface area. Potential measurements via scanning Kelvin probe microscopy (SKPM) used an MFP-3D-Bio-inverted optical microscope system with an ARC2 controller (Asylum Research, Oxford Instruments). The images were recorded by SKPM in NAP mode with a two-pass method. On the first path, the cantilever was oscillated mechanically and the surface topography was recorded, while in the second path, during which AC and DC voltages were applied, the surface potential was recorded. It is important to note that the needle-like structures shown by the Cu_2O−polysaccharide complex in the AFM images were observed only under dry AFM conditions. AFM images were analyzed, and the needle-like structures (spikes) were counted by using Gwyddion and ImageJ software.[52]

Microbial Cultures and Growth Conditions. The antimicrobial and antibiofilm activities of the Cu_2O−polysaccharide complex were tested on a variety of model microorganisms cultured as follows: *Acinetobacter baumannii*, *Escherichia coli*, and *Pseudomonas aeruginosa* PA14 were cultivated for 24 h in Luria−Bertani (LB) Broth (Miller) (Sigma-Aldrich). *Staphylococcus aureus* was grown in BD Tryptic Soy Broth (TSB; soybean-casein digest medium). *Bacillus subtilis* was cultivated in LB medium (Difco Luria−Bertani medium, Lennox). *C. albicans* (ATCC 10231, supplied by the Clinical Microbiology Laboratory of Dr. Yossi Paitan, Meir Medical Center, Kfar Saba) was cultivated in Potato Dextrose Broth (PDB; HiMedia) for 24 h with shaking (120 rpm) at a constant temperature of 37 °C. For the antibiofilm study, *P. aeruginosa* PA14 was inoculated into AB trace Minimal Medium, supplemented with 30 mm glucose at a constant temperature of 37 °C.

Antimicrobial Activity. The antimicrobial activities of the Cu_2O−polysaccharide complex and of the native polysaccharide (in the form of a soft gel) against *A. baumannii*, *P. aeruginosa* PA14, *E. coli*, *S. aureus*, *B. subtilis*, and *C. albicans* were examined by determining the growth curves and viability of the microorganisms. Since Cu_2O is a photoactive material, the experiments were conducted in dark conditions. To determine the growth curves for the different species of bacteria and the fungus, 100 μL of polysaccharide (0.7% w/v), Cu_2O−polysaccharide complex (0.7% w/v polysaccharide with 500 ppm of copper ions), or Cu_2O (500 ppm copper ions) solution was mixed with 900 μL of suitable medium and 10 μL of microbial culture at OD = 1. A sample of 200 μL of each combination was incubated with shaking in 96-well plates at 37 °C for 14 h for *A. baumannii*, *P. aeruginosa* PA14, *E. coli*, *S. aureus*, and *B. subtilis* or 48 h for *C. albicans*. The turbidity of the medium was measured hourly with a micro-plate reader (BioTek Instruments) at a wavelength of 600 nm. Growth inhibition was calculated from the following formula

$$\text{inhibitory index (\%)} = \left(1 - \frac{OD_{treatment} - OD_{treatment-blank}}{OD_{control} - OD_{control-blank}}\right) \times 100$$

where $OD_{treatment}$ is the absorbance of the sample of the Cu_2O−polysaccharide complex or polysaccharide plus bacteria at t = 14 h (in the logarithmic phase of growth) or fungus at t = 48 h, $OD_{treatment\_blank}$ is the absorbance of the same sample without bacteria or fungus at the same time, $OD_{control}$ is the absorbance of only LB or TSB (as mentioned above for each bacteria) and bacteria or PDB and fungus, and $OD_{control\_blank}$ is the absorbance of the same sample without bacteria or fungus at the same time. For cell viability determination, cells were incubated in test tubes containing 900 μL of LB, TSB, or PDB, as relevant, mixed with 100 μL of the Cu_2O−polysaccharide solution (0.7% w/v polysaccharide with 500 ppm copper ions) versus their respective controls (LB, TSB, or PDB alone or solutions of polysaccharide or copper ions). After 24 h, 100 μL of each sample was plated on an LB, TSB, or PDB agar plate after serial dilution and incubated overnight at 37 °C (under dark conditions). On the following morning, CFUs were counted.

Antibiofilm Activity. The morphological properties of the coatings and the biofilm structure were analyzed using SEM. Imaged biofilms of *P. aeruginosa* PA14 and *C. albicans* on Cu_2O-polysaccharide, polysaccharide, and Cu_2O surfaces were acquired using high-resolution (HR)-SEM. After 24 h of incubation, the samples were prepared for SEM studies as follows. After fixation in 2.5% buffered glutaraldehyde, the samples were subsequently dehydrated via an increasing serial ethanol gradient and immersed in a hexamethyldisilazane (HMDS)/ethanol gradient solution (25, 50, 75, 90, 95, and 100%). The treated specimens were air-dried for 4 h and in preparation for SEM scanning (JSM-7400F, JEOL), they were sputter-coated with a 20 nm layer of gold using an EMITECH K575× sputtering device (Emitech Ltd, UK).

https://dx.doi.org/10.1021/acsami.0c17919
ACS Appl. Mater. Interfaces XXXX, XXX, XXX−XXX

Statistical Analysis. Means ± deviations (SD) from triplicate end point data were presented in all tables. Differences between the control and samples were determined using one-way analysis of variance (ANOVA) and the Tuckey post hoc test with GraphPad Prism 6 for Windows software. Statistically significant differences were set at $p < 0.05$.

RESULTS AND DISCUSSION

Chemical and Rheological Characterization of the Cu_2O–Polysaccharide Complex. The first step in studying the complexation of the *Porphyridium* sp. polysaccharide with Cu_2O (pI = 7.5) was to characterize Cu_2O–polysaccharide complexes differing in their Cu_2O contents by using chemical and physical approaches. Table 1 summarizes the relationship between the concentration of added Cu [from 0 ppm (native polysaccharide) to 750 ppm] on the viscosity, conductivity, and zeta potential of the Cu_2O–polysaccharide complexes. All three parameters increased with increasing Cu concentrations, with the viscosity and conductivity rising markedly and the zeta potential less so. Since Cu_2O will dissociate to give Cu ions at the acidic pH of the polysaccharide (pH = 4.5–5.0), the increases in viscosity can probably be attributed to charge screening by the added Cu ions of the unentangled regimes where the polysaccharide chains are not sufficiently close, one to the other, to interact by the formation of H-bonds between the chains as was previously shown in polyelectrolyte solutions.[55] The higher conductivities (up to 181% increase) of the Cu_2O–polysaccharide complexes versus the native polysaccharide were probably due to the higher number of charged particles (Cu ions and polysaccharide). Our results showed that the native polysaccharide and the Cu_2O–polysaccharide complexes exhibited similar values of the zeta potential (range of −45 to −49 mV), implying good stability[56] and probable complexation of Cu ions into the polysaccharide. The zeta potential of the Cu_2O solutions (250/500/750 ppm Cu in buffer, pH 4.5) ranged from +20.5 to +22.9 as was previously described by Guillaume Salek et al.[57] In addition, cyclic voltammetry analysis (Figure S1) of the Cu_2O–polysaccharide complex showed that the oxidation state of copper does not change while in the complex, as was previously indicated.[58] Since all three Cu_2O–polysaccharide complexes exhibited higher viscosities and conductivities than the native polysaccharide and similar zeta potentials to that of the native polysaccharide, we decided to further develop and characterize the complex containing 500 ppm copper and 0.7% of the polysaccharide.

The dynamic viscoelastic properties of the polysaccharide and the Cu_2O–polysaccharide complex were characterized in terms of the frequency dependence of the storage modulus $G'(\omega)$ and the loss modulus $G''(\omega)$ (Figure S2). The results obtained suggest weak gel behavior only for the polysaccharide solution (but not for solutions of the complex), in agreement with previous studies showing that a 1% (w/v) solution of polysaccharide behaves as a weak gel.[18,59] The shift of the crossover position in the Cu_2O–polysaccharide complex to lower than the measurable range (<0.1 rad/s) indicated a longer relaxation time of the chains and demonstrated that the solution behavior of the complex resembled that of a soft gel.

Spectrophotometric and Microscopic Analysis of the Cu_2O–Polysaccharide Complex. Absorption coefficient spectra were used to determine whether there had indeed been a reaction between the polysaccharide and Cu_2O. To this end, spectra of the absorption coefficients derived from the transmittance and reflectance spectra of the Cu_2O–polysaccharide complex were compared to the spectra of the unmixed constituents, that is, polysaccharide and Cu_2O (Figure S3). The difference between the measured and calculated curves for Cu_2O suggests that some reaction did occur between the polysaccharide and Cu_2O.

Similarly, the luminescence behaviors of solutions of the Cu_2O–polysaccharide complex and the polysaccharide were significantly different from that of the Cu_2O solution, with the latter solution exhibiting low luminescence intensity (Figure S4). The main difference between the spectra of the polysaccharide and the Cu_2O–polysaccharide complex was observed in the infra-red range of the spectrum, manifested as a rise in the photoluminescence intensity of the complex at wavelengths longer than 800 nm. This rise may be attributed to the contribution of the added Cu_2O since a similar rise was also observed in the photoluminescence spectrum of the Cu_2O alone.

To elucidate how the copper binds to the polysaccharide, FT-IR spectroscopy was used (Figure 1). The transmission

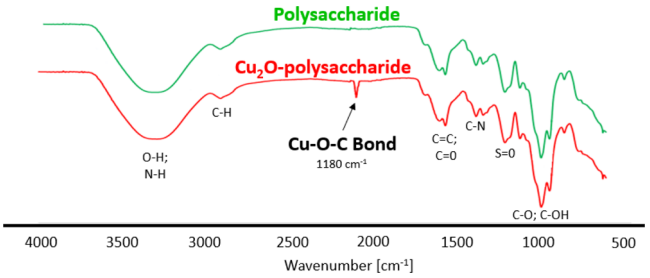

Figure 1. FT-IR transmission spectra of the polysaccharide and the Cu_2O–polysaccharide complex in the region of 650–4000 cm^{-1}. The Cu_2O–polysaccharide complex contained 0.7% polysaccharide (w/v) and 500 ppm copper. To facilitate ease of viewing, the spectra are displaced with respect to the *Y* axis.

spectrum of the Cu_2O–polysaccharide complex differed from that of the polysaccharide in that the former exhibited a new peak at 1180 cm^{-1}, suggesting the formation of a new covalent bond, as has previously been shown.[60,61] In both spectra (Cu_2O–polysaccharide complex and polysaccharide), the broad band centered at 3260 cm^{-1} was assigned to O–H stretching vibrations and the weak signal at 2926 cm^{-1} to C–H stretching vibrations.[62] Both the polysaccharide and the Cu_2O–polysaccharide complex also exhibited a broad band at around 1220–1260 cm^{-1}, which was assigned to sulfated ester groups (S=O)—also a characteristic component of the sulfated polysaccharides of other microalgae and indeed of other algae such as alginate in brown seaweeds.[63−65]

The surface morphologies of the polysaccharide and the Cu_2O–polysaccharide complex were studied by SEM (Figure 2A,B). As can be seen from Figure 2, the structure of the polysaccharide is porous and fibrous. Differences can be seen in the quantity and in the size of the pores between the polysaccharide and the Cu_2O–polysaccharide complex, with the complex having fewer entanglements and larger pores. In addition, in corroboration with the AFM results (see below), the Cu_2O–polysaccharide complex showed a distinct morphology with bright, uniformly scattered needle-like structures (spikes). EDS—used to analyze the chemical compositions of the Cu_2O–polysaccharide complex and the polysaccharide—showed five peaks corresponding to five major elements

https://dx.doi.org/10.1021/acsami.0c17919
ACS Appl. Mater. Interfaces XXXX, XXX, XXX−XXX

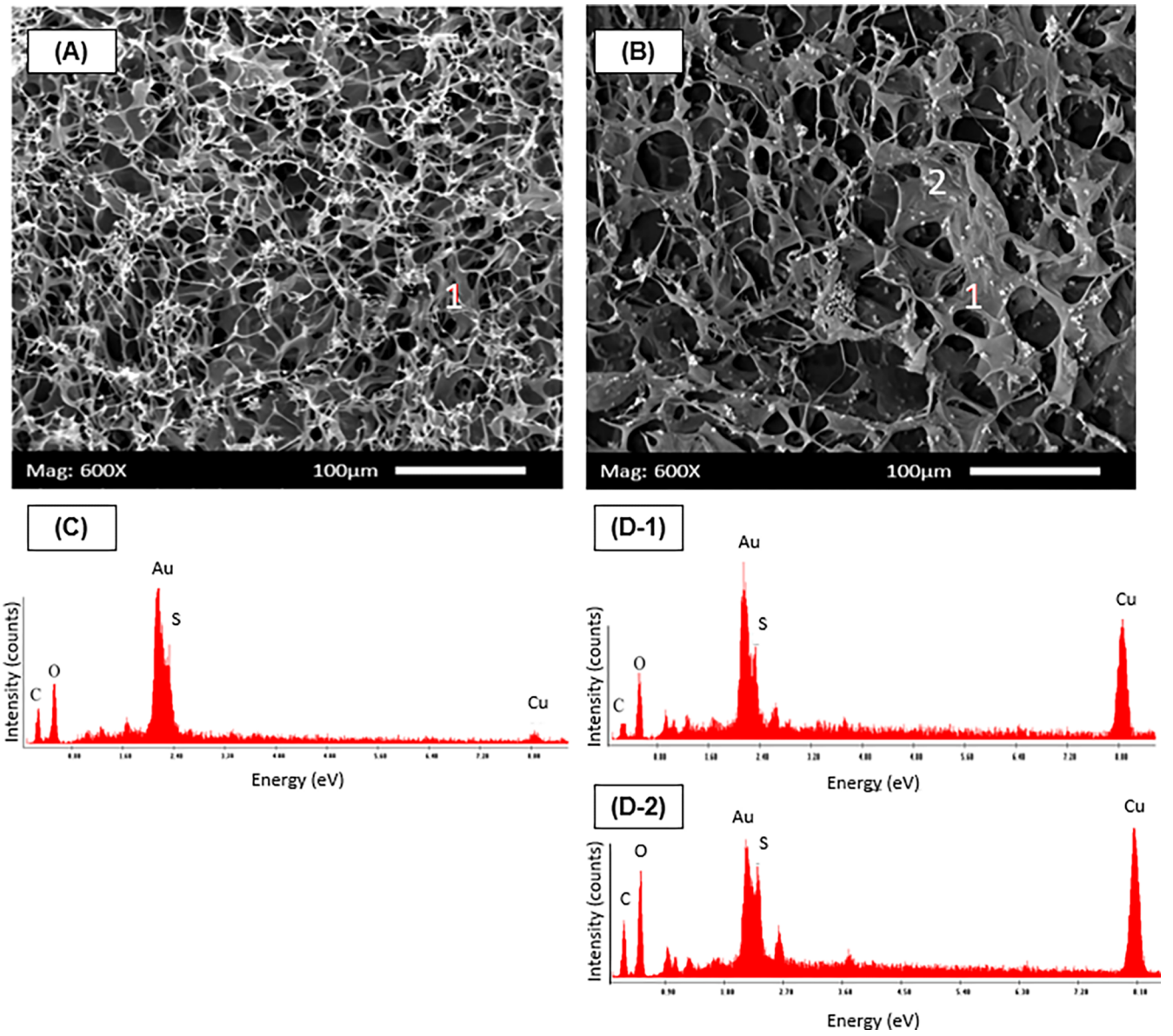

Figure 2. (A,B) SEM micrographs of samples containing (A) 0.7% polysaccharide (w/v) alone and (B) the Cu_2O−polysaccharide complex. (C,D) EDS spectra of (C) of the polysaccharide sample (at area 1); (D1) of the smooth area of the Cu_2O−polysaccharide complex; and (D2) of the grainy area of the Cu_2O−polysaccharide complex (spikes; area 2). For SEM, the samples were freeze-dried and coated with gold; magnification ×600. The Cu_2O−polysaccharide complex contained 500 ppm of copper.

(Figure 2C,D), with the dominant gold peak being due to the gold coating. The main elements identified in the polysaccharide sample were carbon [61.87% (w/v)] and oxygen [30.87% (w/v)], as is to be expected for a sugar-containing polymer. In addition, sulfur [5.57% (w/v)] and small traces of copper [1.69% (w/v)], probably originating from the growth medium (which contains microelements including copper), were also evident. Figure 2D shows the elemental composition of the Cu_2O−polysaccharide complex detected by EDS (1—of the smooth area and 2—of the grainy area, i.e., the spikes, as seen in Figure 2B). Figure 2D-1 shows the elemental composition of the Cu_2O−polysaccharide complex detected by EDS. Again, the main elements identified in this sample were carbon [48.86% (w/v)] and oxygen [31.95% (w/v)] and a small amount of sulfur [8.06% (w/v)]. The main elements identified in the spikes (Figure 2D-2) were carbon [46.44% (w/v)] and oxygen [26.78% (w/v)] and a small amount of sulfur [12.53% (w/v)], indicating that the spikes were derived from the polysaccharide. As expected, the quantity of copper in the complex [11.13−14.24% (w/v)] was significantly higher than that in the polysaccharide. We assume here that the Cu is located on the surface of the complex.

To further study the surface topography and morphology of the Cu_2O−polysaccharide complex, AFM was used (Figure 3). The polysaccharide sample exhibited a generally smooth surface, but with some roughness throughout, that is, the raised structures were approximately 24.16−40.5 nm high and 1−10 nm wide. In contrast, the surface of the Cu_2O−polysaccharide complex was characterized by needle-like structures—spikes—that protruded up to 1000 nm above the surface and had a thickness of approximately 10−20 nm (Figure 3). The above morphologies were similar to those previously described for polysaccharide and Cu−polysaccharide complexes.[14] Using both Gwyddion and ImageJ software,

https://dx.doi.org/10.1021/acsami.0c17919
ACS Appl. Mater. Interfaces XXXX, XXX, XXX−XXX

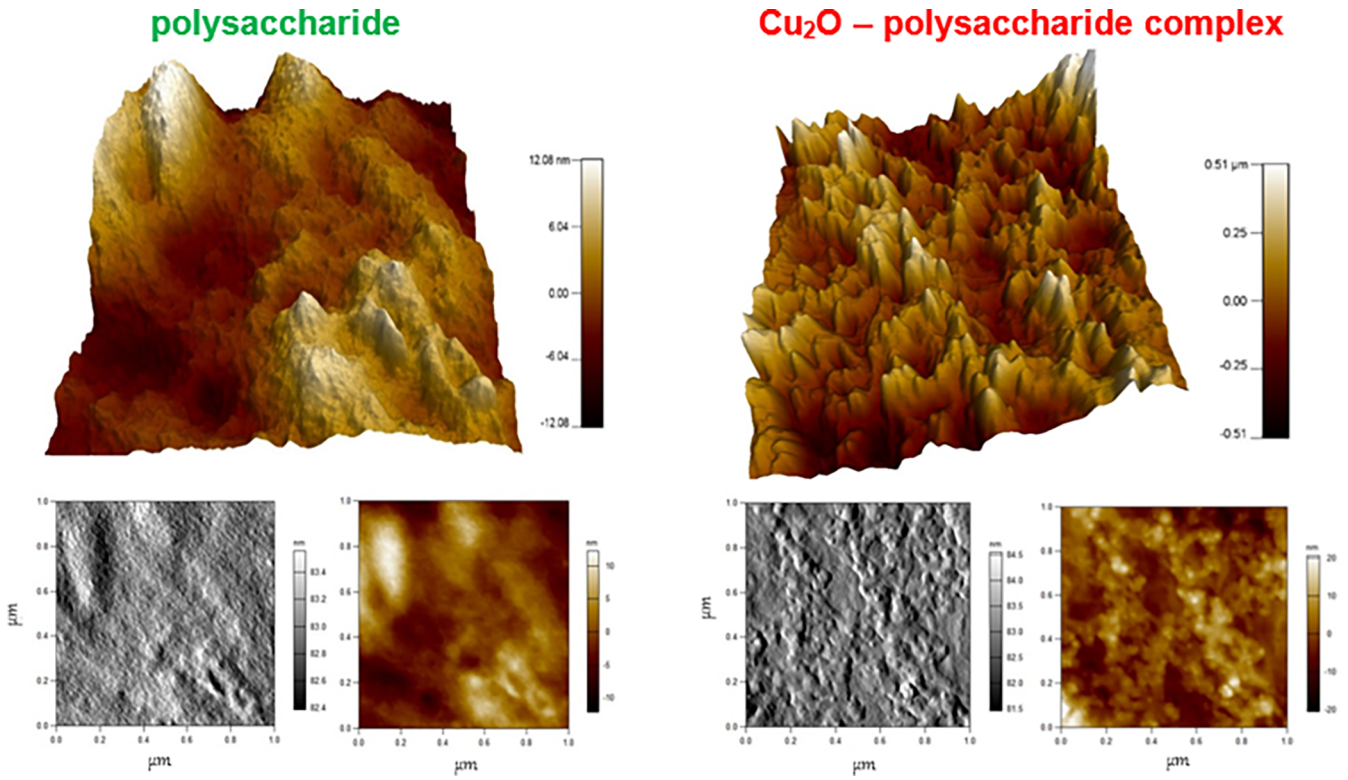

Figure 3. AFM surface topography and 3D images of the polysaccharide and the Cu_2O−polysaccharide complex showing the smooth surface of the polysaccharide and the needle-like structures of the Cu_2O−polysaccharide complex. The Cu_2O−polysaccharide complex contained 0.7% (w/v) polysaccharide and 500 ppm copper.

Table 2. Effect of the Cu_2O−Polysaccharide Complex on the Inhibition of Growth of *C. albicans*, *A. baumannii*, *P. aeruginosa*, *E. coli*, *S. aureus*, and *B. subtilis*[a]

		% inhibition with:		
time of exposure	microorganism	polysaccharide	Cu_2O	Cu_2O−polysaccharide
48 h	*C. albicans*	35.8± 1.2	14.7± 1.9	91.7± 0.4
14 h	*A. baumannii*	40.1± 3.5	9.7± 2.9	78.5± 9.8
14 h	*P. aeruginosa*	45.9± 0.9	4.9± 6.5	78.1± 5.1
14 h	*E. coli*	49.2± 4.1	1.6± 1.8	75.0± 1.5
14 h	*S. aureus*	30.8± 5.6	20.9± 8.9	72.9± 7.1
14 h	*B. subtilis*	29.6± 2.9	15.6± 2.7	79.7± 2.5

[a]The Cu_2O−polysaccharide complex contained 0.07% (w/v) polysaccharide and 30 ppm copper. Values in the table are means ± SD of three different experiments performed in triplicate.

the number of the spikes on the Cu_2O−polysaccharide complex surface was counted[52] and found to be about 5000 ± 400 spikes/μm^2.

The above findings are in agreement with other studies showing that nano-topography spikes influence microbial viability after adhesion of a "nano-spiked" material to microbial cells as was previously shown for *E. coli*.[42] and in *Saccharomyces cerevisiae*.[43] It has also been shown that the rigidity of the microbial cells affect their susceptibility to mechanical rupture,[41,44,51] for example, Gram-negative bacteria were more sensitive than Gram-positive bacteria, probably due to the cell wall architecture.[66,67] Finally, it has been shown that the increased spike density and greater spike height promote the efficacy of the antimicrobial activity of the "nano-spiked" material.[41−51] However, the precise mechanism leading to microbial cell death is not fully understood.

Antimicrobial Activity of the Cu_2O−Polysaccharide Complex. The antimicrobial activity of the Cu_2O−polysaccharide complex was evaluated (using turbidity measurements) in various model microbial pathogens, namely, the fungus *C. albicans* (generation time 82 min), the Gram-negative bacteria *A. baumannii* (generation time 48 min), *P. aeruginosa PA14* (generation time 35 min), and *E. coli* (generation time 21 min), and the Gram-positive bacteria, *S. aureus* (generation time 30 min), and *B. subtilis* (generation time 28 min) (Table 2). Because of the dilution process of the assay (as described in the Experimental section), the final concentration of copper was 30 ppm, and polysaccharide concentration was 0.07% (w/v). The Cu_2O−polysaccharide complex almost completely inhibited the growth of *C. albicans* (91.7 ± 0.4% inhibition as compared with untreated cells), whereas Cu_2O alone exhibited low activity (about 15% inhibition), as previously reported for Cu_2O activity.[68] The polysaccharide alone exhibited moderate activity in inhibiting *C. albicans* (35.8 ± 1.2% inhibition). For the various bacterial species, the Cu_2O−polysaccharide complex exhibited 72−78%

https://dx.doi.org/10.1021/acsami.0c17919
ACS Appl. Mater. Interfaces XXXX, XXX, XXX−XXX

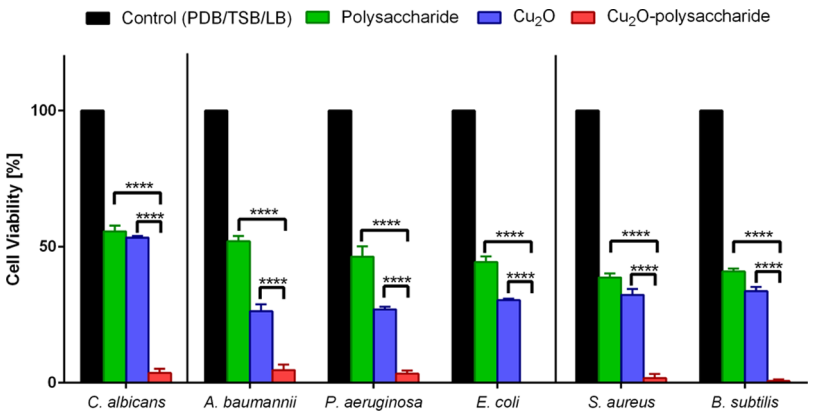

Figure 4. Effect of the Cu_2O–polysaccharide complex on the cell viability of *C. albicans*, *A. baumannii*, *P. aeruginosa*, *E. coli*, *S. aureus*, and *B. subtilis* cultures. The Cu_2O–polysaccharide complex contained 0.07% (w/v) polysaccharide and 30 ppm copper. Values are the average of triplicate determinations. With the Anova test, all the results were significant compared to the control ($p < 0.05$). PDB, TSB, LB.

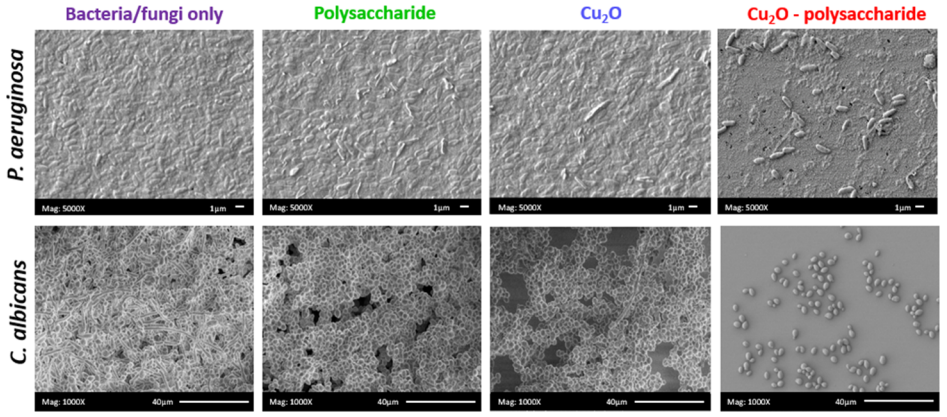

Figure 5. HR-SEM images of the Cu_2O–polysaccharide complex, polysaccharide, and Cu_2O surfaces in biofilm assays against *C. albicans* and *Pseudomonas aeruginosa* PA14. The microorganisms growing on clean glass surfaces served as the control. The Cu_2O–polysaccharide complex contained 0.7% (w/v) polysaccharide and 500 ppm copper.

inhibition. Cu_2O alone did not inhibit bacterial growth, and the polysaccharide alone demonstrated only moderate inhibition (reduction of about 30–49% in growth for the bacteria, respectively, as compared with untreated cells). This difference in inhibitory activity between the Gram-negative and the Gram-positive bacteria may be due to their different cell wall compositions and structures.[69]

To investigate the bactericidal effect of the Cu_2O–polysaccharide complex, the viability of the fungal and bacterial cells was determined in a CFU assay. Cells were inoculated on agar plates and allowed to grow at 37 °C. After an overnight incubation with the Cu_2O–polysaccharide complex or its controls (growth medium alone or polysaccharide or Cu_2O solutions alone), CFUs were counted and cell viability was determined in comparison with the control values (growth medium plus polysaccharide or Cu_2O). The results show that the most effective treatment against *C. albicans* was that of the Cu_2O–polysaccharide complex (Figure 4), with about 3% viable cells after the treatment as compared with ∼45% viable cells with polysaccharide alone or the copper oxide alone. Similarly, low cell viabilities were previously reported for Cu_2O.[70,71] For all bacteria, no or minimal bacterial growth was detected. Thus, it seems that the Cu_2O–polysaccharide complex not only inhibited fungal and bacterial growth but also caused cell death. A few studies have reported on the activity of Cu_2O against bacteria and fungi. One of those studies showed relatively high antifungal activity of Cu_2O–Cu nanoparticles/alginate (30 ppm Cu) against *Neoscytalidium dimidiatum*, but only after a long incubation period of 8 days.[24] In a different study, an additive effect was found for chitosan-copper against *C. albicans*, *Candida parapsilosis*, *E.coli*, and *P. aeruginosa* when higher copper concentrations were used (>1000 ppm).[72] Relatively high activity was also observed with PET/Cu_2O@ZrP nanosheets having a high Cu content (186,200 ppm) against *S. aureus*, *E. coli*, and *C. albicans*.[73]

In summary, it is evident that the antifungal and antibacterial activities of the Cu_2O–polysaccharide complex are more potent than those of the polysaccharide or Cu_2O alone. The viability test also showed that the Cu_2O–polysaccharide complex not only inhibited microbial growth but also reduced the number of viable cells. The low inhibitory effects of the polysaccharide alone against all the investigated bacterial species (*A. baumannii*, *P. aeruginosa* PA14, *E. coli*, *S. aureus*, and *B. subtilis*) might result from mass transport limitation of nutrients to the cells. The strongest effect was obtained for the Cu_2O–polysaccharide complex, which caused 91% inhibition of *C. albicans* growth after 48 h and 97% cell death after 24 h. It seems that the antimicrobial potency of the Cu_2O–polysaccharide complex versus the polysaccharide or Cu_2O alone is probably due to the spikes on the surface of the Cu_2O–polysaccharide complex.

https://dx.doi.org/10.1021/acsami.0c17919
ACS Appl. Mater. Interfaces XXXX, XXX, XXX–XXX

To investigate the antibiofilm activity of the Cu_2O–polysaccharide complex, *C. albicans* and *P. aeruginosa* PA14, used as model pathogens, were grown on clean glass surfaces in the presence and absence (as the control) of the Cu_2O–polysaccharide complex or the polysaccharide or Cu_2O alone. The Cu_2O–polysaccharide complex (dehydrated) on the glass surface demonstrated significantly improved microbial clearance as compared to a polysaccharide film and Cu_2O alone (Figure 5). In response to the Cu_2O–polysaccharide complex treatment, only a few individual cells were observed. Antibiofilm activity was less evident on the surface treated with the polysaccharide or Cu_2O alone (Figure 5).

CONCLUSIONS

In this study, we undertook a physicochemical and bioactivity characterization of a Cu_2O–polysaccharide complex. It was shown (by FT-IR) that in the Cu_2O–polysaccharide complex, the Cu ions were covalently bound to the polysaccharide. The complex exhibited higher viscosity and conductivity than the native polysaccharide, but zeta-potential and rheological properties were similar. Similarly, the complex displayed a porous fibrous structure and weak-gel-like behavior, similar to the native polysaccharide.

The Cu_2O–polysaccharide complex was effective against various microorganisms as compared to the polysaccharide or Cu alone. It almost completely inhibited *C. albicans* (91% inhibition) and presented significant inhibitory activity of biofilm formation against bacteria (*P. aeruginosa*) and fungi (*C. albicans*) as was seen in SEM images. The Cu_2O–polysaccharide complex was characterized by needle-like topographical protrusions (on AFM), which leads us to the conclusion that these structures are related to the complex's antimicrobial and antibiofilm activities. Although the EDS-SEM studies indicated the existence of Cu on the surface of the complex, probably responsible for a cationic charge localized on the complex surface, the main antimicrobial effect may be attributed to the modified surface topography of the Cu_2O–polysaccharide complex, that is, to the spikes 1000 nm in height and 10–20 nm in width, at a density of about 5000 spikes/μm^2. It seems likely that the high density of the spikes coupled with their height can cause mechanical penetration of the microbial membrane, leading to disruption of membrane permeability and consequently to cell death, as has been shown previously.[41−51]

The sulfated polysaccharide of *Porphyridium* sp. was used here as a platform for the incorporation of Cu_2O. The surface of the Cu_2O–polysaccharide complex was dramatically modified, yielding a new surface topography and hence new bioactivities. These results encourage further development of the unique Cu–polysaccharide complex as well as other metal–polysaccharide combinations toward the development of additional metal–polysaccharide complexes with potential antibacterial and fungicidal activities.

ASSOCIATED CONTENT

Supporting Information

The Supporting Information is available free of charge at https://pubs.acs.org/doi/10.1021/acsami.0c17919.

Cyclic voltammogram of the Cu_2O–polysaccharide complex in acetonitrile; mechanical spectrum of the polysaccharide and the Cu_2O–polysaccharide complex; absorption coefficient spectra of polysaccharide, Cu_2O–polysaccharide complex, and Cu_2O alone versus wavelength; and photoluminescence spectra of the polysaccharide, Cu_2O–polysaccharide complex, and Cu_2O (PDF)

AUTHOR INFORMATION

Corresponding Author

Shoshana (Malis) Arad − *Avram and Stella Goldstein-Goren Department of Biotechnology Engineering, Ben-Gurion University of the Negev, Beer-Sheva 8410501, Israel;* orcid.org/0000-0002-6356-8440; Email: arad@post.bgu.ac.il

Authors

Nofar Yehuda − *Avram and Stella Goldstein-Goren Department of Biotechnology Engineering, Ben-Gurion University of the Negev, Beer-Sheva 8410501, Israel*

Yury Turkulets − *Department of Electrical and Computer Engineering, Ben-Gurion University of the Negev, Beer-Sheva 8410501, Israel*

Ilan Shalish − *Department of Electrical and Computer Engineering, Ben-Gurion University of the Negev, Beer-Sheva 8410501, Israel*

Ariel Kushmaro − *Avram and Stella Goldstein-Goren Department of Biotechnology Engineering, Ben-Gurion University of the Negev, Beer-Sheva 8410501, Israel; The Ilse Katz Center for Meso and Nanoscale Science and Technology, Ben-Gurion University of the Negev, Beer-Sheva 8410501, Israel*

Complete contact information is available at: https://pubs.acs.org/10.1021/acsami.0c17919

Notes

The authors declare no competing financial interest.

REFERENCES

(1) Gantt, E.; Edwards, M. R.; Conti, S. F. Ultrastructure of Porphyridium aerugineum a Blue-Green Colored Rhodophytan. *J. Phycol.* **1968**, *4*, 65−71.

(2) Sommerfeld, M. R.; Nichols, H. W. Comparative Studies in the Genus Porphyridium Naeg. *J. Phycol.* **1970**, *6*, 67−78.

(3) Jones, R. F.; Speer, H. L.; Kury, W. Studies on the Growth of the Red Alga Porphyridium cruentum. *Physiol. Plant.* **1963**, *16*, 636−643.

(4) Ramus, J.; Groves, S. T. Incorporation of Sulfate into the Capsular Polysaccharide of the Red Alga Porphyridium. *J. Cell Biol.* **1972**, *54*, 399−407.

(5) Geresh, S.; Arad, S. The Extracellular Polysaccharides of the Red Microalgae: Chemistry and Rheology. *Bioresour. Technol.* **1991**, *38*, 195−201.

(6) Lupescu, N.; Arad, S.; Geresh, S.; Bernstein, M. A.; Glaser, R. Structure of Some Sulfated Sugars Isolated after Acid Hydrolysis of the Extracellular Polysaccharide of Porphyridium sp., a Unicellular Red Alga. *Carbohydr. Res.* **1991**, *210*, 349−352.

(7) Arad, S. M.; van Moppes, D. Novel sulfated polysaccharides of red microalgae: Basics and applications. *Handbook of Microalgal Culture: Applied Phycology and Biotechnology*; Wiley Online Library, 2013; pp 406−416.

(8) Arad (Malis), S.; Levy-Ontman, O. Sulfated Polysaccharides in the Cell Wall of Red Microalgae. *Handbook of Biopolymer-Based Materials: From Blends and Composites to Gels and Complex Networks*; Wiley Online Library, 2013; pp 351−370.

(9) Arad (Malis), S. Production of the Sulfated Polysacchrides from Red Unicellular Algae. *Algal Biotechnol.* Stadler, T., Mollion, J., Verdus, M-C., Karamanos, Y., Morvan, H., Christiaen, D., Eds. Elsevier Applied Science, London, 1988, *1*, 65−87.

(10) Krzesłowska, M. The Cell Wall in Plant Cell Response to Trace Metals: Polysaccharide Remodeling and Its Role in Defense Strategy. *Acta Physiol. Plant.* **2011**, *33*, 35−51.
(11) Huleihel, M.; Ishanu, V.; Tal, J.; Arad, S. Antiviral Effect of Red Microalgal Polysaccharides on Herpes simplex and Varicella zoster Viruses. *J. Appl. Phycol.* **2001**, *13*, 127−134.
(12) Matsui, M. S.; Muizzuddin, N.; Arad, S.; Marenus, K. Sulfated Polysaccharides from Red Microalgae Have Antiinflammatory Properties in vitro and in vivo. *Appl. Biochem. Biotechnol., Part A* **2003**, *104*, 13.
(13) Tannin-Spitz, T.; Bergman, M.; Van-Moppes, D.; Grossman, S.; Arad, S. Antioxidant Activity of the Polysaccharide of the Red Microalga Porphyridium sp. *J. Appl. Phycol.* **2005**, *17*, 215−222.
(14) Golberg, K.; Emuna, N.; Vinod, T. P.; Van Moppes, D.; Marks, R. S.; Arad, S. M.; Kushmaro, A. Novel Anti-Adhesive Biomaterial Patches: Preventing Biofilm with Metal Complex Films (MCF) Derived from a Microalgal Polysaccharide. *Adv. Mater. Interfaces* **2016**, *3*, 1500486.
(15) Arad, S.; Rapoport, L.; Moshkovich, A.; Van Moppes, D.; Karpasas, M.; Golan, R.; Golan, Y. Superior Biolubricant from a Species of Red Microalga. *Langmuir* **2006**, *22*, 7313−7317.
(16) Geresh, S.; Arad, S.; Shefer, A. Chemically Crosslinked Polysaccharide of the Red MicroalgaRhodella Reticulata- An Ion Exchanger for Toxic Metal Ions1. *J. Carbohydr. Chem.* **1997**, *16*, 703−708.
(17) Ramus, J.; Kenney, B. E.; Shaughnessy, E. J. Drag Reducing Properties of Microalgal Exopolymers. *Biotechnol. Bioeng.* **1989**, *33*, 550−557.
(18) Netanel Liberman, G.; Ochbaum, G.; Arad, S.; Bitton, R. The Sulfated Polysaccharide from a Marine Red Microalga as a Platform for the Incorporation of Zinc Ions. *Carbohydr. Polym.* **2016**, *152*, 658−664.
(19) Vincent, M.; Duval, R. E.; Hartemann, P.; Engels-Deutsch, M. Contact Killing and Antimicrobial Properties of Copper. *J. Appl. Microbiol.* **2018**, *124*, 1032−1046.
(20) Amelia Piñón Castillo, H.; Nayzzel Muñoz Castellanos, L.; Martínez Chamorro, R.; Reyes Martínez, R.; Orrantia Borunda, E. Nanoparticles as New Therapeutic Agents against *Candida albicans*. In Candida albicans. **2019**. DOI: 10.5772/intechopen.80379.
(21) El-Batal, A. I.; El-Sayyad, G. S.; Mosallam, F. M.; Fathy, R. M. Penicillium Chrysogenum-Mediated Mycogenic Synthesis of Copper Oxide Nanoparticles Using Gamma Rays for in vitro Antimicrobial Activity Against Some Plant Pathogens. *J. Cluster Sci.* **2020**, *31*, 79−90.
(22) Rani, H.; Singh, S. P.; Yadav, T. P.; Khan, M. S.; Ansari, M. I.; Singh, A. K. In-Vitro Catalytic, Antimicrobial and Antioxidant Activities of Bioengineered Copper Quantum Dots Using Mangifera indica (L.) Leaf Extract. *Mater. Chem. Phys.* **2020**, *239*, 122052.
(23) Festa, R. A.; Jones, M. B.; Butler-Wu, S.; Sinsimer, D.; Gerads, R.; Bishai, W. R.; Peterson, S. N.; Darwin, K. H. A novel copper-responsive regulon in Mycobacterium tuberculosis. *Mol. Microbiol.* **2011**, *79*, 133−148.
(24) Applerot, G.; Lellouche, J.; Lipovsky, A.; Nitzan, Y.; Lubart, R.; Gedanken, A.; Banin, E. Understanding the Antibacterial Mechanism of CuO Nanoparticles: Revealing the Route of Induced Oxidative Stress. *Small* **2012**, *8*, 3326−3337.
(25) Yang, Z.; Ma, C.; Wang, W.; Zhang, M.; Hao, X.; Chen, S. Fabrication of Cu2O-Ag nanocomposites with enhanced durability and bactericidal activity. *J. Colloid Interface Sci.* **2019**, *557*, 156−167.
(26) Du, B. D.; Ngoc, D. T. B.; Thang, N. D.; Tuan, L. N. A.; Thach, B. D.; Hien, N. Q. Synthesis and in vitro antifungal efficiency of alginate-stabilized Cu2 O-Cu nanoparticles against Neoscytalidium dimidiatum causing brown spot disease on dragon fruit plants (Hylocereus undatus). *Vietnam J. Chem.* **2019**, *57*, 318−323.
(27) SI, A.; Pal, K.; Kralj, S.; El-Sayyad, G. S.; de Souza, F. G.; Narayanan, T. Sustainable Preparation of Gold Nanoparticles via Green Chemistry Approach for Biogenic Applications. *Mater. Today Chem.* **2020**, *17*, 100327.
(28) Bhardwaj, B.; Singh, P.; Kumar, A.; Kumar, S.; Budhwar, V. Eco-Friendly Greener Synthesis of Nanoparticles. *Adv. Pharm. Bull.* **2020**, *10*, 566−576.
(29) Rajeshkumar, S.; Sekar, D.; Ezhilarasan, D.; Lakshmi, T. The Role of Diverse Nanoparticles in Oxidative Stress: In vitro and in vivo Studies. *Role of Oxidative Stress in Pathophysiology of Diseases*; Springer, 2020; pp 27−48.
(30) Zhang, Y.; Hudson-Smith, N. V.; Frand, S. D.; Cahill, M. S.; Davis, L. S.; Feng, Z. V.; Haynes, C. L.; Hamers, R. J. Influence of the Spatial Distribution of Cationic Functional Groups at Nanoparticle Surfaces on Bacterial Viability and Membrane Interactions. *J. Am. Chem. Soc.* **2020**, *142*, 10814−10823.
(31) Al-Awady, M. J.; Greenway, G. M.; Paunov, V. N. Nanotoxicity of Polyelectrolyte-Functionalized Titania Nanoparticles towards Microalgae and Yeast: Role of the Particle Concentration, Size and Surface Charge. *RSC Adv.* **2015**, *5*, 37044−37059.
(32) Halbus, A. F.; Horozov, T. S.; Paunov, V. N. Colloid Particle Formulations for Antimicrobial Applications. *Adv. Colloid Interface Sci.* **2017**, *249*, 134−148.
(33) Meikle, T. G.; Dyett, B. P.; Strachan, J. B.; White, J.; Drummond, C. J.; Conn, C. E. Preparation, Characterization, and Antimicrobial Activity of Cubosome Encapsulated Metal Nanocrystals. *ACS Appl. Mater. Interfaces* **2020**, *12*, 6944−6954.
(34) Uma, B.; Anantharaju, K. S.; Renuka, L.; Nagabhushana, H.; Malini, S.; More, S. S.; Vidya, Y. S.; Meena, S. Controlled synthesis of $(CuO\text{-}Cu_2O)Cu/ZnO$ multi oxide nanocomposites by facile combustion route: A potential photocatalytic, antimicrobial and anticancer activity. *Ceram. Int.* **2020**, DOI: 10.1016/j.ceramint.2020.09.223.
(35) Perreault, F.; Oukarroum, A.; Melegari, S. P.; Matias, W. G.; Popovic, R. Polymer Coating of Copper Oxide Nanoparticles Increases Nanoparticles Uptake and Toxicity in the Green Alga Chlamydomonas reinhardtii. *Chemosphere* **2012**, *87*, 1388−1394.
(36) Quaranta, D.; Krans, T.; Santo, C. E.; Elowsky, C. G.; Domaille, D. W.; Chang, C. J.; Grass, G. Mechanisms of Contact-Mediated Killing of Yeast Cells on Dry Metallic Copper Surfaces. *Appl. Environ. Microbiol.* **2011**, *77*, 416−426.
(37) Usman, M. S.; El Zowalaty, M. E.; Shameli, K.; Zainuddin, N.; Salama, M.; Ibrahim, N. A. Synthesis, Characterization, and Antimicrobial Properties of Copper Nanoparticles. *Int. J. Nanomed.* **2013**, *8*, 4467−4479.
(38) Mahapatra, O.; Bhagat, M.; Gopalakrishnan, C.; Arunachalam, K. D. Ultrafine Dispersed CuO Nanoparticles and Their Antibacterial Activity. *J. Exp. Nanosci.* **2008**, *3*, 185−193.
(39) Lazary, A.; Weinberg, I.; Vatine, J.-J.; Jefidoff, A.; Bardenstein, R.; Borkow, G.; Ohana, N. Reduction of Healthcare-Associated Infections in a Long-Term Care Brain Injury Ward by Replacing Regular Linens with Biocidal Copper Oxide Impregnated Linens. *Int. J. Infect. Dis.* **2014**, *24*, 23−29.
(40) Besold, A. N.; Culbertson, E. M.; Culotta, V. C. The Yin and Yang of Copper during Infection. *J. Biol. Inorg Chem.* **2016**, *21*, 137−144.
(41) Jenkins, J.; Mantell, J.; Neal, C.; Gholinia, A.; Verkade, P.; Nobbs, A. H.; Su, B. Antibacterial Effects of Nanopillar Surfaces Are Mediated by Cell Impedance, Penetration and Induction of Oxidative Stress. *Nat. Commun.* **2020**, *11*, 1626.
(42) Bandara, C. D.; Singh, S.; Afara, I. O.; Wolff, A.; Tesfamichael, T.; Ostrikov, K.; Oloyede, A. Bactericidal Effects of Natural Nanotopography of Dragonfly Wing onEscherichia coli. *ACS Appl. Mater. Interfaces* **2017**, *9*, 6746−6760.
(43) Nowlin, K.; Boseman, A.; Covell, A.; Lajeunesse, D. Adhesion-Dependent Rupturing of Saccharomyces cerevisiae on Biological Antimicrobial Nanostructured Surfaces. *J. R. Soc., Interface* **2015**, *12*, 20140999.
(44) Elbourne, A.; Chapman, J.; Gelmi, A.; Cozzolino, D.; Crawford, R. J.; Truong, V. K. Bacterial-Nanostructure Interactions: The Role of Cell Elasticity and Adhesion Forces. *J. Colloid Interface Sci.* **2019**, *546*, 192−210.

https://dx.doi.org/10.1021/acsami.0c17919
ACS Appl. Mater. Interfaces XXXX, XXX, XXX−XXX

(45) Arias, S. L.; Devorkin, J.; Spear, J. C.; Civantos, A.; Allain, J. P. Bacterial Envelope Damage Inflicted by Bioinspired Nanospikes Grown in a Hydrogel. *ACS Appl. Bio Mater.* **2020**, *3*, 7974−7988.
(46) Li, L.; He, J.; Hu, H.; Tian, F.; Chang, H.; Zhang, J.; Wang, C.; Rao, W. Interactions of Bacteria With Monolithic Lateral Silicon Nanospikes Inside a Microfluidic Channel. *Front. Chem.* **2019**, *7*, 483.
(47) Park, S.; Park, H.-H.; Sun, K.; Gwon, Y.; Seong, M.; Kim, S.; Park, T.-E.; Hyun, H.; Choung, Y.-H.; Kim, J.; Jeong, H. E. Hydrogel Nanospike Patch as a Flexible Anti-Pathogenic Scaffold for Regulating Stem Cell Behavior. *ACS Nano* **2019**, *13*, 11181.
(48) Tripathy, A.; Sen, P.; Su, B.; Briscoe, W. H. Natural and Bioinspired Nanostructured Bactericidal Surfaces. *Advances in Colloid and Interface Science*. Elsevier B.V. 2017, *248*, pp 85−104. DOI: 10.1016/j.cis.2017.07.030.
(49) Linklater, D. P.; Juodkazis, S.; Rubanov, S.; Ivanova, E. P. Comment on "Bactericidal Effects of Natural Nanotopography of Dragonfly Wing on Escherichia coli". *ACS Appl. Mater. Interfaces* **2017**, *9*, 29387.
(50) Kelleher, S. M.; Habimana, O.; Lawler, J.; O' Reilly, B.; Daniels, S.; Casey, E.; Cowley, A. Cicada Wing Surface Topography: An Investigation into the Bactericidal Properties of Nanostructural Features. *ACS Appl. Mater. Interfaces* **2016**, *8*, 14966−14974.
(51) Crawford, R. J.; Webb, H. K.; Truong, V. K.; Hasan, J.; Ivanova, E. P. Surface Topographical Factors Influencing Bacterial Attachment. *Adv. Colloid Interface Sci.* **2012**, *179*−*182*, 142−149.
(52) Elbourne, A.; Coyle, V. E.; Truong, V. K.; Sabri, Y. M.; Kandjani, A. E.; Bhargava, S. K.; Ivanova, E. P.; Crawford, R. J. Multi-Directional Electrodeposited Gold Nanospikes for Antibacterial Surface Applications. *Nanoscale Adv.* **2019**, *1*, 203−212.
(53) Cohen, E.; Arad, S. A Closed System for Outdoor Cultivation of Porphyridium. *Biomass* **1989**, *18*, 59−67.
(54) Dubois, M.; Gilles, K. A.; Hamilton, J. K.; Rebers, P. A.; Smith, F. *Colorimetric Method for Determination of Sugars and Related Substances*; ACS Publications, 1956.
(55) Wyatt, N. B.; Gunther, C. M.; Liberatore, M. W. Increasing Viscosity in Entangled Polyelectrolyte Solutions by the Addition of Salt. *Polymer* **2011**, *52*, 2437−2444.
(56) Matusiak, J.; Grządka, E. Stability of Colloidal Systems - a Review of the Stability Measurements Methods. *Ann. Univ. Mariae Curie-Sklodowska, Sect. AA: Chem.* **2017**, *72*, 33.
(57) Salek, G.; Tenailleau, C.; Dufour, P.; Guillemet-Fritsch, S.; Guillemet, S.; Salek, G.; Tenailleau, C.; Dufour, P.; Guillemet-Fritsch, S. Room temperature inorganic polycondensation of oxide (Cu2O and ZnO) nanoparticles and thin films preparation by the dip-coating technique. *Thin Solid Films* **2015**, *589*, 872−876.
(58) Fekri, R.; Salehi, M.; Asadi, A.; Kubicki, M. DNA/BSA Interaction, Bio-Activity, Molecular Docking Simulation Study and Electrochemical Properties of Hydrazone Schiff Base Derived Cu(II)/Ni(II) Metal Complexes: Influence of the Nuclearity and Metal Ions. *Polyhedron* **2017**, *128*, 175−187.
(59) Eteshola, E.; Karpasas, M.; Arad, S.; Gottlieb, M. Red Microalga Exopolysaccharides: 2. Study of the Rheology, Morphology and Thermal Gelation of Aqueous Preparations. *Acta Polym.* **1998**, *49*, 549−556.
(60) Padil, V. V. T.; Černík, M. Green Synthesis of Copper Oxide Nanoparticles Using Gum Karaya as a Biotemplate and Their Antibacterial Application. *Int. J. Nanomed.* **2013**, *8*, 889.
(61) Akerlof *Infrared Spectral Interpetation A Systematic Approach*. Smith, B. C., CRC Press LLC, 1970; Vol. *53*.
(62) Gómez-Ordóñez, E.; Rupérez, P. FTIR-ATR Spectroscopy as a Tool for Polysaccharide Identification in Edible Brown and Red Seaweeds. *Food Hydrocolloids* **2011**, *25*, 1514−1520.
(63) Leal, D.; Matsuhiro, B.; Rossi, M.; Caruso, F. FT-IR Spectra of Alginic Acid Block Fractions in Three Species of Brown Seaweeds. *Carbohydr. Res.* **2008**, *343*, 308−316.
(64) Rupérez, P. Mineral Content of Edible Marine Seaweeds. *Food Chem.* **2002**, *79*, 23−26.
(65) Synytsya, A.; Kim, W.-J.; Kim, S.-M.; Pohl, R.; Synytsya, A.; Kvasnička, F.; Čopíková, J.; Il Park, Y. Structure and Antitumour Activity of Fucoidan Isolated from Sporophyll of Korean Brown Seaweed Undaria Pinnatifida. *Carbohydr. Polym.* **2010**, *81*, 41−48.
(66) Hazell, G.; Fisher, L. E.; Murray, W. A.; Nobbs, A. H.; Su, B. Bioinspired Bactericidal Surfaces with Polymer Nanocone Arrays. *J. Colloid Interface Sci.* **2018**, *528*, 389−399.
(67) Silhavy, T. J.; Kahne, D.; Walker, S. The Bacterial Cell Envelope. *Cold Spring Harbor Perspectives in Biology*; Cold Spring Harbor Lab, 2010.
(68) Padmavathi, A. R.; Priya, S.; Das, A.; Priya, A.; Sushmitha, T. J.; Pandian, S. K.; Toleti, S. R. Impediment to growth and yeast-to-hyphae transition in Candida albicans by copper oxide nanoparticles. *Biofouling* **2020**, *36*, 56−72.
(69) Raposo, M. F. D. J.; De Morais, A. M. M. B.; De Morais, R. M. S. C. Influence of Sulphate on the Composition and Antibacterial and Antiviral Properties of the Exopolysaccharide from Porphyridium cruentum. *Life Sci.* **2014**, *101*, 56−63.
(70) Shahmiri, M.; Ibrahim, N. A.; Shayesteh, F.; Asim, N.; Motallebi, N. Preparation of PVP-coated copper oxide nanosheets as antibacterial and antifungal agents. *J. Mater. Res.* **2013**, *28*, 3109.
(71) Zhou, J.; Xiang, H.; Zabihi, F.; Yu, S.; Sun, B.; Zhu, M. Intriguing anti-superbug Cu_2O@ZrP hybrid nanosheet with enhanced antibacterial performance and weak cytotoxicity. *Nano Res.* **2019**, *12*, 1453−1460.
(72) Wang, X.; Du, Y.; Fan, L.; Liu, H.; Hu, Y. Chitosan- metal complexes as antimicrobial agent: Synthesis, characterization and Structure-activity study. *Polym. Bull.* **2005**, *55*, 105−113.
(73) Zhou, J.; Fei, X.; Li, C.; Yu, S.; Hu, Z.; Xiang, H.; Sun, B.; Zhu, M. Integrating Nano-Cu2O@ZrP into In Situ Polymerized Polyethylene Terephthalate (PET) Fibers with Enhanced Mechanical Properties and Antibacterial Activities. *Polymers* **2019**, *11*, 113.

https://dx.doi.org/10.1021/acsami.0c17919
ACS Appl. Mater. Interfaces XXXX, XXX, XXX−XXX